JOURNAL OF COMPUTATIONAL PHYSICS 89, 207–240 (1990)

A New Lagrangian Method for Steady Supersonic Flow Computation I. Godunov Scheme

C. Y. LOH AND W. H. HUI

Department of Applied Mathematics, Unniversity of Waterloo, Waterloo, Ontario, Canada N2L 3G1

Received October 19, 1988; revised August 4, 1989

This paper studies the problem of steady two-dimensional supersonic flow of an inviscid compressible fluid using the new Lagrangian formulation of Hui and Van Roessel, in which the stream function and the Lagrangian time are used as independent variables. A shock capturing method is developed by applying the first-order Godunov scheme to the conservation form equations of this formulation. The method is fast and robust. Furthermore, extensive comparisons with exact solutions and with the second-order Godunov scheme of Glaz and Wardlaw based on the Eulerian formulation show that the first-order Lagrangian method generally attains the same level of accuracy as the second-order Eulerian method and is even better in resolving slip line discontinuities.

I. INTRODUCTION

The numerical simulation of inviscid compressible flow as modelled by the Euler equations of gas dynamics is of theoretical as well as practical importance. Over the past four decades numerous techniques have been devised to tackle the difficulty of representing the shock and slip line (or contact line) discontinuities which are the dominant features of the flow. The three major approaches—namely, artificial viscosity, blending of low and high order accurate fluxes, and Godunov-type of using nonlinear solutions to the Riemann's problem—have been critically evaluated and compared in the excellent review article of Woodward and Collella [1], especially for two-dimensioal flow with strong shocks. A more recent survey of the methods of treating shocks and vortex sheets can also be found in [2].

It appears from [1, 2] that most existing works, with the exception of one-dimensional flow, are based on the Eulerian method of description of fluid motion. Although in several important papers such as [3–5] some steps of computation based on Lagrangian method are also used, these are always followed by a remap step from a Lagrangian grid back to the original Eulerian one.

Most existing works of Godunov-type for two-dimensional flow also use the method of time-splitting and arrive at a steady flow as an asymptotic state of the unsteady flow after marching a large number of time steps. In the case of supersonic flow a direct attack on the steady Euler equations is also possible, as they are of

0021-9991/90 $3.00

hyperbolic type and a "time-like" variable can be identified. This has the clear advantage of reducing the number of independent variables immediately by one, thus rendering the (steady) two-dimensional problem to that similar to the one-dimensional unsteady flow. Glaz Wardlaw [6] are the first to have successfully developed such a direct steady flow computational scheme based on the Eulerian formulation. The purpose of this paper is to develop an alternative method by using the new Lagrangian formulation of Hui and Van Roessel [7].

The motivation of the present work stems from the important observation of Woodward and Collella [1] that "the overall accuracy of such (numerical) simulations is very closely related to the accuracy with which flow discontinuities are represented." The new Lagrangian formulation, by virtue of its use of streamlines and time lines as coordinate lines, is expected to provide a basis for better (than Eulerian) representation of the slip line (contact line) discontinuities. This expectation turns out to be well confirmed, and the new Lagrangian formulation, together with the Godunov scheme, appears to have advantages over the Eulerian one, and have the potential of accurately simulating steady and unsteady inviscid compressible flow of gas dynamics with relative ease of efforts.

In Section II the new Lagrangian formulation is described briefly, which forms the theoretical basis for the application of Godunov scheme in Section III. Several test examples are given in Section IV and compared extensively with the exact solutions and with the results of Glaz and Wardlaw [6] using Eulerian formulation. Finally, discussions of the new Lagrangian method and conclusions are given in Section V.

II. The New Lagrangian Formulation

It is well known that there exist two basic methods of specifying fluid motion: the Eulerian and the Lagrangian. Although one-dimensional unsteady flow and problems of free boundaries composed of same set of fluid particles are often studied routinely and preferably using Lagrangian formulation, most of the theoretical and numerical studies of fluid flow are based on the Eulerian one. In particular, the latter clearly enjoys an advantage over the conventional Lagrangian one for steady flow in that the time variable t disappears so that the number of independent variables is immediately reduced from four to three in the Eulerian formulation, wheras the conventional Lagrangian formulation apparently still needs four independent variables.[1]

Recently, Hui and Van Roessel [7] have introduced a Lagrangian time τ which plays a dual role of the Lagrangian label of a fluid particle while being the time of

[1] It might be argued that these four apparently independent variables must, for steady flow, satisfy an integral relation and thus, only three of them are truly independent. This is indeed correct. However, such a relation is not known a priori but, rather, is solution-dependent. So it cannot be used easily to eliminate one of the four independent variables explicitly.

motion. In this way the number of independent variables for steady flow is also immediately reduced from four to three, placing the new Lagrangian formulation on the same ground as the Eulerian one even for steady flow. Furthermore, the difference between Lagrangian time τ and Eulerian time t in unsteady flow can be exploited to render the free boundary problem of flow with a shock wave a fixed boundary one. It has been used to solve succesfully the problem of hypersonic flow past three dimensional shapes [8, 9].

We shall briefly derive the new Lagrangian formulation for steady three dimensional flow from the Eulerian formulation of motion of an inviscid, non-heat conducting perfect gas obeying the γ-law. The equations of motion are

$$\nabla \cdot (\rho \mathbf{V}) = 0 \tag{1}$$

$$\mathbf{V} \cdot \nabla \mathbf{V} + \nabla p/\rho = 0 \tag{2}$$

$$\mathbf{V} \cdot \nabla (p/\rho^{\gamma}) = 0, \tag{3}$$

where as usual, $\mathbf{V}$ denotes the velocity vector, p the pressure, ρ the density, and γ the ratio of specific heats of the gas.

First, the continuity equation (1) is eliminated by the use of two stream functions ξ and η,

$$\rho \mathbf{V} = K(\xi, \eta) \nabla \xi \times \nabla \eta \tag{4}$$

or, equivalently,

$$\rho v^i = K(\xi, \eta) \varepsilon^{ijk} \frac{\partial \xi}{\partial x^j} \frac{\partial \eta}{\partial x^k}, \tag{5}$$

where x^i $(i = 1, 2, 3)$ (or x, y, z) are cartesian coordinates, v^i (or u, v, w) the corresponding components of velocity, ε^{ijk} is the permutation symbol, and K is an arbitrary function of ξ and η. Second, a function τ is introduced via

$$\frac{\partial(\tau, \xi, \eta)}{\partial(x^1, x^2, x^3)} = \frac{\rho}{K(\xi, \eta)} \equiv \frac{1}{J}. \tag{6}$$

We now make the coordinate transformation from (x^1, x^2, x^3) to (τ, ξ, η) and regard the latter as independent variables. Then, by inversion we get

$$\frac{\partial x^i}{\partial \tau} = \varepsilon^{ijk} \frac{\partial \xi}{\partial x^j} \frac{\partial \eta}{\partial x^k} J = v^i \qquad (i = 1, 2, 3) \tag{7}$$

and hence the material derivative

$$\frac{D}{Dt} = v^i \frac{\partial}{\partial x^i} = \frac{\partial x^i}{\partial \tau} \frac{\partial}{\partial x^i} = \frac{\partial}{\partial \tau}. \tag{8}$$

Equations (7) and (8) clearly show that the function τ introduced above is the time

of motion in the new Lagrangian formulation using (τ, ξ, η) as independent variables, and hence the name Lagrangian time. It plays the dual role of being the time of motion and, jointly with the stream functions, of labelling fluid particles. This places the new Lagrangian formulation on the same ground as the Eulerian one for steady flow in that it, too, requires only three independent variables.

Under the transformation, the Euler equations (1)–(3) become

$$K\frac{\partial u}{\partial \tau}+\frac{\partial(p, y, z)}{\partial(\tau, \xi, \eta)}=0 \tag{9}$$

$$K\frac{\partial v}{\partial \tau}+\frac{\partial(x, p, z)}{\partial(\tau, \xi, \eta)}=0 \tag{10}$$

$$K\frac{\partial w}{\partial \tau}+\frac{\partial(x, y, p)}{\partial(\tau, \xi, \eta)}=0 \tag{11}$$

$$\frac{K}{\rho}=\frac{\partial(x, y, z)}{\partial(\tau, \xi, \eta)} \tag{12}$$

$$\frac{p}{\rho^{\gamma}}=S(\xi, \eta). \tag{13}$$

In the special case of two-dimensional flow, only one stream function, ξ, say, is needed and the governing equations simplify to

$$K(\xi)\frac{\partial u}{\partial \tau}+\frac{\partial(p, y)}{\partial(\tau, \xi)}=0 \tag{14}$$

$$K(\xi)\frac{\partial v}{\partial \tau}+\frac{\partial(x, p)}{\partial(\tau, \xi)}=0 \tag{15}$$

$$\frac{K(\xi)}{\rho}=\frac{\partial(x, y)}{\partial(\tau, \xi)} \tag{16}$$

$$\frac{p}{\rho^{\gamma}}=S(\xi). \tag{17}$$

Let

$$U=\frac{\partial x}{\partial \xi} \tag{18a}$$

$$V=\frac{\partial y}{\partial \xi} \tag{18b}$$

$$H=\frac{1}{2}(u^2+v^2)+\frac{\gamma}{\gamma-1}\frac{p}{\rho} \tag{19}$$

then from (16)

$$K = \rho(uV - vU). \tag{20}$$

The system (14)–(17) may then be written in conservation form

$$\frac{\partial \mathbf{E}}{\partial \tau} + \frac{\partial \mathbf{F}}{\partial \xi} = 0, \tag{21}$$

where

$$\mathbf{E} = \begin{pmatrix} K \\ H \\ Ku + pV \\ Kv - pU \\ U \\ V \end{pmatrix} \equiv \begin{pmatrix} e_1 \\ e_2 \\ e_3 \\ e_4 \\ e_5 \\ e_6 \end{pmatrix}, \qquad \mathbf{F} = \begin{pmatrix} 0 \\ 0 \\ -pv \\ pu \\ -u \\ -v \end{pmatrix}. \tag{22}$$

The first four equations in (21) can, of course, also be derived directly from the physical laws of conservation of mass, energy, and momentum respectively, whereas the last two equations arise from the compatibility conditions between the τ-derivatives (7) and the ξ-derivatives (18), of x and y. Equations (21) in conservation form will be used in Section III for shock capturing based on the Godunov scheme.

In the new Lagrangian formulation the coordinate lines are the streamlines and the time lines. Consequently, the flow tangency condition on a solid boundary is satisfied exactly on a coordinate line, $\xi = \xi_0$, say. We further remark that, since slip lines are also streamlines, they must be coordinate lines. This makes it possible to resolve slip lines better than Eulerian formulation. Furthermore, the streamlines and time lines possess much of the physics of the flow and are easily observable experimentally as they both are material lines.

III. Application of Godunov Scheme

For supersonic flow, the Mach number $M = [\rho(u^2 + v^2)/\gamma p]^{1/2} > 1$ everywhere in the flow field so the system (21), or equivalently, the system (14)–(17), is of hyperbolic type. With the conservation system (21), one can, in principle, apply different types of shock-capturing schemes, such as the sophisticated TVD or ENO (see, e.g., [10, 11]) schemes. As a first exploration of the potential of the new Lagrangian formulation, we apply the standard (first-order) Godunov scheme to (21) in a manner similar to that for one-dimensional unsteady flow.

The computational domain in the $\tau - \xi$ plane is illustrated in Fig. 1. A rectangular mesh is used and the computation marches in the Lagrangian time τ. The

superscript n refers to the time step number and subscript j refers to the cell number. The marching step, $\Delta\tau^n = \tau^{n+1} - \tau^n$, is uniform for all j. It may vary with n but is always so chosen as to satisfy the usual CFL linear stability condition. The mesh divides the computational domain into control volumes or cells which in the ξ-direction are centered at (τ^n, ξ_j) and have a height of $\Delta\xi_j = \xi_{j+1/2} - \xi_{j-1/2}$ (for all n). Unless otherwise stated, we shall use uniform cell width so that $\Delta\xi_j = h$ for all j.

The difference equations for the jth cell at time step n are formally derived by integrating (21) over the shaded rectangle in Fig. 1 and applying the divergence theorem. The result is

$$\mathbf{E}_j^{n+1} = \mathbf{E}_j^n - \frac{\Delta\tau^n}{\Delta\xi_j}\left(\mathbf{F}_{j+1/2}^{n+1/2} - \mathbf{F}_{j-1/2}^{n+1/2}\right). \tag{23}$$

Here for any quantity f,

$$f_j^n = \frac{1}{\Delta\xi_j}\int_{\xi_{j-1/2}}^{\xi_{j+1/2}} f(\tau^n, \xi)\, d\xi \tag{24}$$

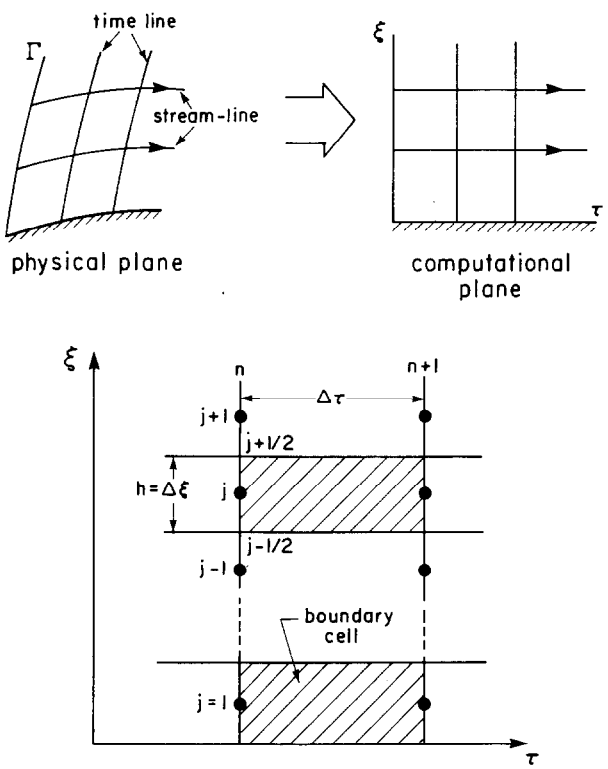

FIG. 1. Computational domain and mesh.

is the cell-average of f and

$$f_{j+1/2}^{n+1/2} = \frac{1}{\Delta\tau^n} \int_{\tau^n}^{\tau^{n+1}} f(\tau, \xi_{j+1/2})\, d\tau \tag{25}$$

is its time-average.

In the first-order Godunov scheme the jth-cell average, $\mathbf{E}_j^n$, at time n is considered as constant within that cell and the flux $\mathbf{F}_{j+1/2}^{n+1/2}$ along the interface (a streamline) between the jth cell and the $(j+1)$th cell from time step n to $n+1$ is to be obtained from the self-similar solution $\mathbf{R}((\xi - \xi_{j+1/2})/(\tau - \tau^n); \mathbf{Q}_j^n, \mathbf{Q}_{j+1}^n)$ at $\xi = \xi_{j+1/2}$ to the Riemann problem formed by two adjacent constant flow states $\mathbf{Q}_j^n$ and $\mathbf{Q}_{j+1}^n$, where $\mathbf{Q} = (p, \rho, u, v)^{\mathrm{T}}$. The solution to the Riemann problem yields a flow consisting of the well-known Prandtl–Meyer expansion flow and the oblique shock and slip line discontinuities. However, no special consideration is needed for slip lines as they are also streamlines in steady flow. A Newton iterative method is employed (see Appendix A) for solving the Riemann problem. It has fast convergence; usually only two to four iterations are needed to achieve an accuracy of 10^{-6} even in the severe cases.

To sum up, the numerical procedures are as follows:

Step 1. *Initiation.* Given a flow problem in the Eulerian $x-y$ plane, we choose a line Γ, not itself a streamline, where the flow is known (e.g., a given uniform flow), and identify it as the time line $\tau = 0$ in the Lagrangian $\tau - \xi$ plane. We then parameterize Γ by the stream function ξ (for instance, we take ξ equal to the arc length of Γ) and lay a grid $\xi_0, \xi_1, ..., \xi_N$ on Γ. Hence along $\tau = 0$, U^0, V^0, as well as the flow $\mathbf{Q}^0$ are known as initial conditions. In all test examples in this paper we take the line $\tau = 0$ perpendicular to the given uniform flow as Γ and choose ξ to be the arc length of Γ. This results in $U_j^0 = 0$, $V_j^0 = 1$. $\mathbf{E}_j^0$ are then known at $\tau = 0$ for all j by taking average within the cell.

Step 2. With all $\mathbf{E}_j^n$ and $\mathbf{Q}_j^n$ known at time step n ($n = 0, 1, 2, ...$). We solve the local Riemann problems for all j (see Appendix A) and obtain its solution, $\mathbf{R}(0, \mathbf{Q}_j^n, \mathbf{Q}_{j+1}^n)$, at the cell interfaces (see Appendix A).

Step 3. The flux vectors $\mathbf{F}_{j\pm 1/2}^{n+1/2}$ are then computed according to (25) (or, equivalently, according to (22), as $\mathbf{R}(0, \mathbf{Q}_j^n, \mathbf{Q}_{j+1}^n)$ do not change with τ). Consequently, $\mathbf{E}_j^{n+1}$ are obtained following (23).

Step 4. Finally we decode $\mathbf{E}_j^{n+1}$ to get $\mathbf{Q}_j^{n+1}$ and thus complete the procedure of marching forward in τ by one step. The decoding is rather easy: Let

$$A = \left(\frac{1+\gamma}{1-\gamma}\right)(e_5^2 + e_6^2)$$

$$B = \frac{2}{\gamma - 1}(e_3 e_6 - e_4 e_5)$$

$$C = e_3^2 + e_4^2 - 2K^2 H;$$

then the pressure p satisfies the quadratic equation

$$Ap^2 + Bp + C = 0.$$

It can be shown that $\Delta = B^2 - 4AC \geqslant 0$ and that the appropriate solution for p is

$$p = \frac{-B + \sqrt{\Delta}}{2A}. \tag{26}$$

The other flow variables are

$$u = \frac{e_3 - e_6 p}{K} \tag{27}$$

$$v = \frac{e_4 + e_5 p}{K} \tag{28}$$

$$\rho = \frac{K}{ue_6 - ve_5}. \tag{29}$$

At this stage the numerical procedure is completed. To march forward further in τ, one goes back to Step 2 and repeats Steps 2–4.

If a solid boundary is present in the flow, it must be a streamline and hence can be identified by $\xi = \text{const} = 0$, on which the inclination angle θ is given. The boundary condition to be imposed on the solid boundary is then

$$\frac{v}{u} = \tan \theta_B, \tag{30}$$

where θ_B is the inclination of the solid boundary. This results in a boundary Riemann problem (see Appendix A). As is well known (Glaz and Wardlaw [6], Noh [12], Goodman [13]) a streamline in steady flow is a linearly-degenerate characteristic of the flow along which the boundary condition usually yields poor accuracy at the boundary for the density and Mach number if there is a slope discontinuity at the boundary. A special procedure similar to the one used by Glaz and Wardlaw [6] for boundary conditions are used to significantly improve the accuracy (see examples in Section IV). The details of our special procedure for sudden turns at the body surface are presented in Appendix B.

We remark that the new Lagrangian method is self-contained in the Lagrangian plane $\tau - \xi$ and does not require a remap to go back to Eulerian plane $x - y$ in the process of computation. Such a remap can result in loss of accuracy.

IV. Test Problems

To test the accuracy and robustness of the new Lagrangian method we apply it to several examples and compare the results with the exact solutions and with the second-order Godunov scheme of Glaz and Wardlaw using Eulerian formulation.

We now consider several initial-boundary value problems with or without slope discontinuities on the boundary. In all the cases where there is a corner at the boundary, we take the corner exactly at some time step τ^n, as this is easily done and helps to improve accuracy.

The first example is a uniform supersonic flow with Mach number $M = 3$ passing over a smooth convex parabolic body $b = -\frac{1}{4}x^2$. In this case there is no slope discontinuity on the body surface and the flow is continuous. We use 40 grid points with $h = 0.002$ to compute the expansion flow. Table I presents the computed pressure along the body surface and its exact values, which are obtained through the Riemann invariants. It is seen that the overall relative error is only 0.06%.

The second example is that of a hypersonic stream with Mach number $M = 10$ past a 30° wedge (Fig. 2), where 20 grid points with $h = 0.01$ are used. The computed results are plotted and compared to the exact solution. With the application of boundary conditions (30) on the wedge surface, accurate numerical results are obtained except on the wedge surface where, due to a sudden turn at the wedge apex, larger errors occur in density and Mach number. The same was found by Glaz and Wardlaw [6, Fig. 9] who use a special treatment to remedy it. When their special procedure is adopted to our Lagrangian method (see Appendix B) the large errors in density (and Mach number) near a solid boundary are also eliminated (Fig. 2b) and our first-order Lagrangian method yields results of the same level of accuracy as their second-order Eulerian method. To facilitate more direct comparison with Eulerian results we plot the curves of pressure, density, or Mach number versus the Eulerian co-ordinate y.

In the third example we consider a Prandtl–Meyer flow with $M = 10$ and a 10° turning angle. Here 150 grid points are employed and $h = 0.01$. In a computation without any special procedure the relsults are plotted and compared to the exact ones in Figs. 3a, b. It is seen that near the body surface A' the computed density has poor accuracy. With our special procedure (see Appendix B), which is equivalent to

TABLE I

Surface Pressure and Errors

x	p (computed)	p (exact)	Error	% error
0.005002	0.078529	0.078485	0.000044	0.056
0.025054	0.075077	0.075035	0.000042	0.056
0.050214	0.070921	0.070881	0.000040	0.056
0.075474	0.066940	0.066903	0.000037	0.055
0.100829	0.063131	0.063096	0.000035	0.055
0.126275	0.059492	0.059458	0.000034	0.057
0.151805	0.056020	0.055987	0.000033	0.059
0.177416	0.052709	0.052677	0.000032	0.061
0.203101	0.049558	0.049527	0.000031	0.062

Note. $b = -0.25x^2$, $M = 3$, $h = 0.002$, $\Delta\tau = 0.0005$.

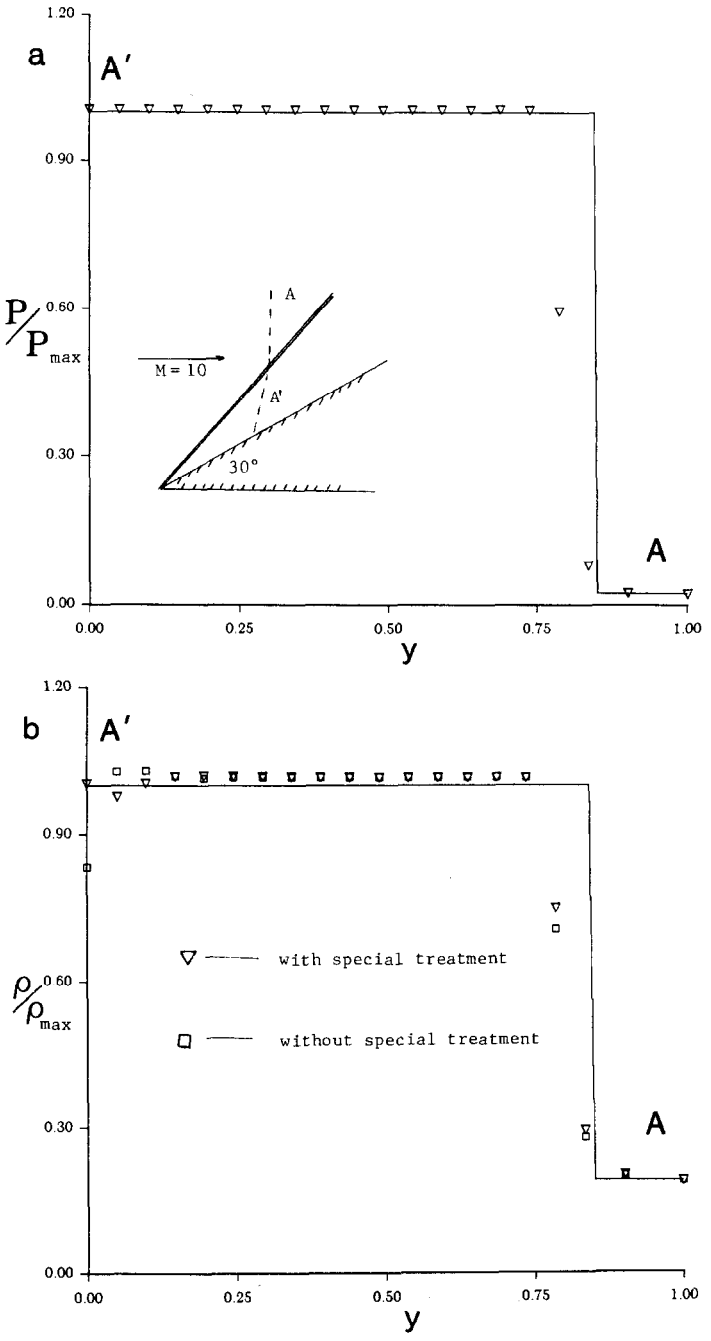

FIG. 2. Flow variables vs Eulerian co-ordinate y (normalized) along time line $A-A'$ ($\tau = 0.875$), solid line denotes the exact solution: (a) pressure; (b) density, with and without special boundary procedure.

imposing an exact solution locally around the sudden turn of the boundary, accuracies are found much improved (Figs. 3c, d) and they are also comparable to that of the second order Eulerian method by Glaz and Wardlaw [6, Fig. 10].

The exact solutions for the wedge flow and the Prandtl–Meyer flow can be expressed either in Eulerian co-ordinates (x, y) or in Lagrangian coo-ordinates (τ, ξ). While the Eulerian version is well known, the Lagrangian version is given in Appendix C.

The fourth example is that of shock interaction of Glaz and Wardlaw [6], which is generated in a converging channel containing both upper and lower wall slope discontinuities (Fig. 4). The collision of the two shocks belonging to different families produces two new shocks and a slip line discontinuity. The exact solution to this problem can be constructed using the oblique shock theory to predict the location and strengths of the shocks induced by the upper and lower wall slope discontinuities. The resulting interaction of these two shocks can be determined exactly by the Riemann solver in Appendix A. Figure 4 illustrates the computed property values at section A–A' and B–B' along with the exact solutions. Figures 4a–c represent the flow upstream of the shock interaction and show the two shocks generated by the upper and lower slope discontinuities, whereas Figs. 4d–f represent the flow downstream of the interaction and show the two resulting shocks as well as a slip line. When comparisons of Fig. 4 with Fig. 17 of Glaz and Wardlaw [6] is made, we see again that our first-order Lagrangian method is just as accurate as their second-order Eulerian method. In fact, the slip line discontinuity is more sharply resolved by the first-order Lagrangian method than the second-order Eulerian method. In this case we use 100 grid points with $h = 0.01$ and apply special procedure to the body slope discontinuities. We also note that due to the mapping effect from the stream function ξ to y the points are distributed unevenly—they are denser in the compression regions than the expansion regions. In addition, as a result of the inaccuracy at the first step of the special procedure, the wall cell points are somewhat away from the other points.

The fifth example is that of interaction shocks of the same family resulting from a supersonic flow past a double wedge (Fig. 5). Here we use 100 grid points with $h = 0.005$ and apply the special procedure to the first corner only. The wedge angles are 10° and 14°, respectively, and the free stream Mach number is 3. The exact solution consists of three parts: the oblique shock solutions for the first and second wedges and the shock collision formed by the free stream flow and the uniform flow behind the second shock. The shock collision is solved exactly by the Riemann solver (Appendix A). Since the two colliding shocks are from the same family, the resultant slip line inclination (24.25°) is very close to that of the uniform flow behind the second shock (24°). This implies that the turning angle in the P-M expansion is only 0.25° and the expansion fan becomes very narrow (see the little "kink" in Fig. 5c at B').

Our numerical results agree well with the theoretical solutions (solid lines). Results on time line $A - A'$ (Figs. 5a, b) represent a typical solution before the shock collision. Two shoks are observed along $A - A'$. Results on time line $B - B'$

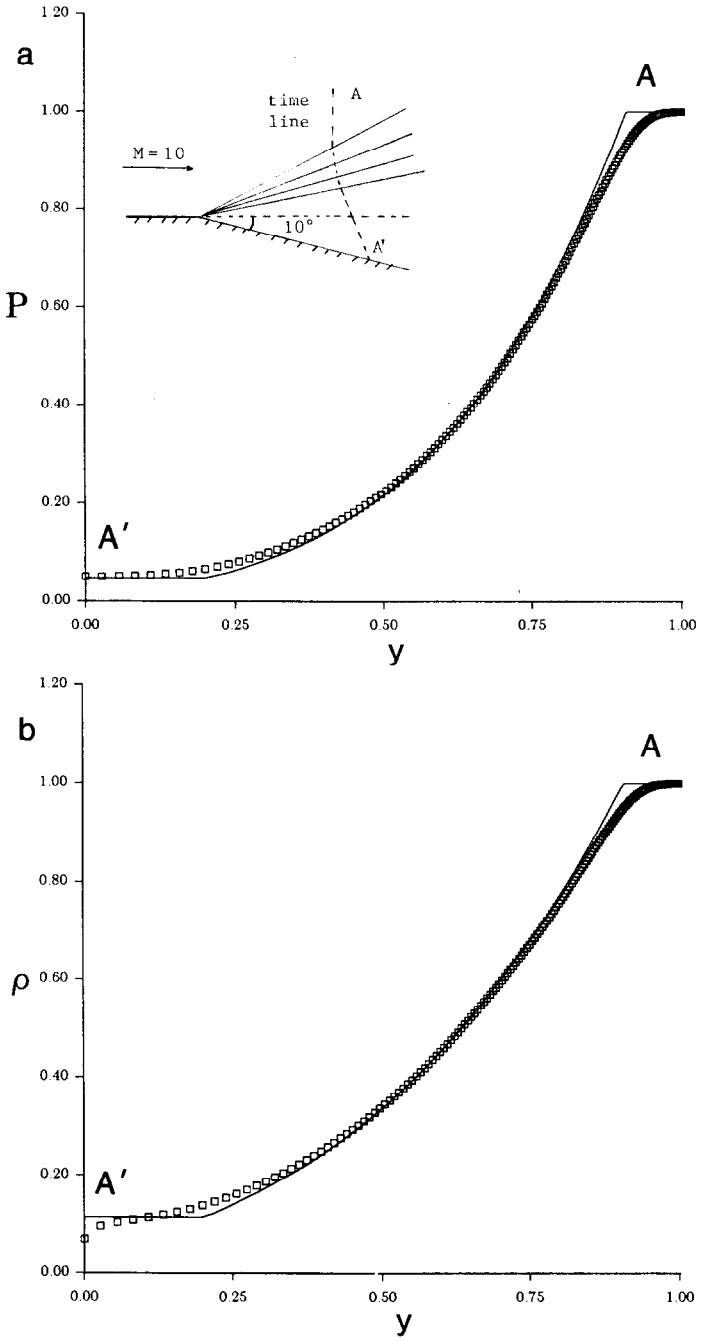

FIG. 3. Flow variables vs Eulerian co-ordinate y (normalized) along time line $A - A'$ ($\tau = 1.0$), solid lines enote exact solution: (a) pressure and (b) density, without special procedure; (c) pressure and (d) density, with special procedure.

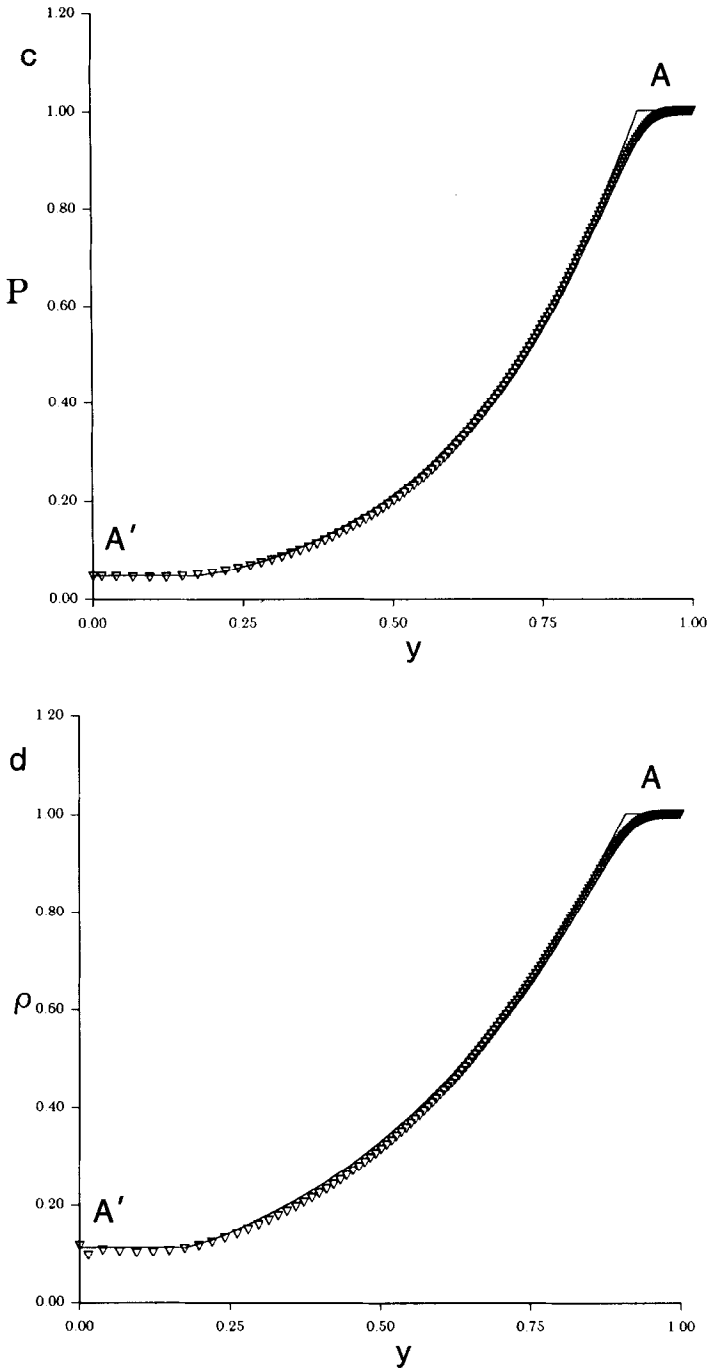

FIGURE 3 (*continued*)

(Figs. 5c, d) represent a typical solution after shock interaction. Here we observe a strong shock and a weak P-M expansion. From Fig. 5c it is seen that around the location B' of the Prandtl–Meyer expansion fan the numerical pressure value does increase slightly.

Now we turn to test our numerical method for the pure initial value problems.

Two Riemann problems are considered in Figs. 6 and 7. Riemman problem No. 1 is formed by the confluence of two parallel streams with different states and is the one used by Glaz and Wardlaw [6]. The ratios in pressure, density, and Mach number across the two streams are 4, 2, and $\frac{5}{3}$, respectively. In the exact solution, the resulting interaction produces an oblique shock adjacent to the low-pressure stream and a Prandtl–Meyer expansion flow on the high-pressure stream side. The resulting density jump across the slip line is $\frac{4}{3}$. Numerical results for the flow properties at section $A-A'$ (a time line) are shown in Fig. 6 along with the exact solution which was generated using the Riemann solver in Appendix A. Comparisons with the Eulerian results of Glaz and Wardlaw [6, Fig. 15] show again that our first-order Lagrangian method attains the same level of accuracy as their second-order Eulerian method in representation of shock and slip line discontinuities. In fact, the slip line discontinuities are better resolved by our first-order Lagrangian method than their second-order Eulerian method. However, our first-order Lagrangian results are less accurate than their second-order Eulerian results for the continuous flow (expansion).

Riemann problem No. 2 formed by two intersecting streams is shown in Fig. 7. Here, the angle of inersection between the streams is 15° while the ratio in pressure, density, and Mach number jumps across the two streams are 10, 5, and 1.5, respectively. This is clearly a more severe case than Riemann problem No. 1, but the resulting interaction produces similar feasures, namely, an oblique shock adjacent to the low-pressure stream and a Prandtl–Meyer expansion flow on the hight-pressure steam side. The Mach number jump across the slip line is 6.7039/2.6118. Numerical results following a time line $\tau = \tau_A$ are shown in Fig. 7 along with the exact solution which was generated using the Riemann solver in Appendix A. Again, it is seen that shock and slip line discontinuities are sharply resolved by the first-order Godunov scheme based on the new Lagrangian formulation.

Finally, we consider the flow past a sharp-nosed body. The free stream Mach number is 3 and the body surface is specified as follows:

$$b = \begin{cases} x^2, & x \leqslant 0.25 \\ 0.0625, & x > 0.25. \end{cases}$$

In the computation we use 120 grid points with $h = 0.006$ uniformly. The time step size $\Delta\tau$ is first chosen to be 0.001 and then reduced to 0.0001 around the shock area. The computed streamlines are presented in Fig. 8a, in which one sees the formation and development of a strong floating shock and the expansion flow downstream of it. A theoretical analysis shows that the floating shock begins at $x = 0.11$ and our picture (Fig. 8) shows that the numerical result is about right. In Fig. 8b we also present the Mach lines of the same flow which show clearly the shape of the shock.

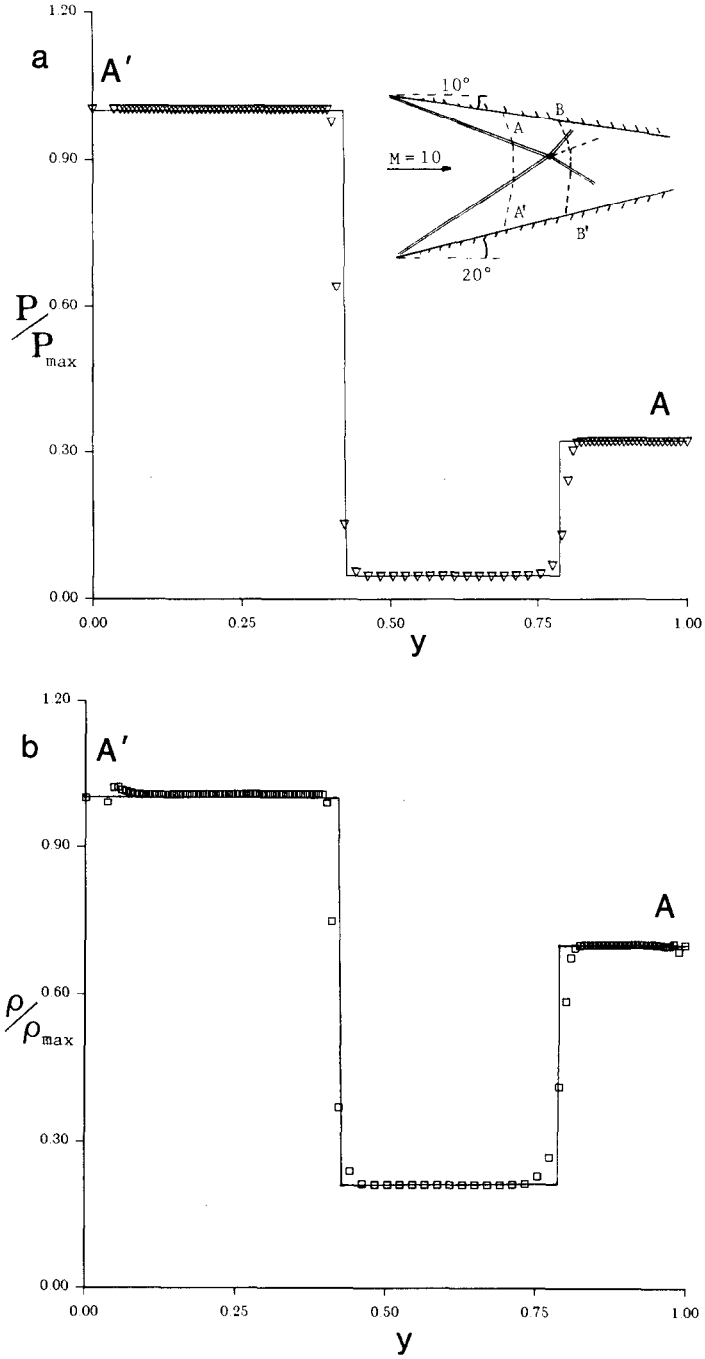

FIG. 4. Flow variables vs Eulerian co-ordiate y (normalized) along time lines before and after the shock interaction, with special procedure at the wedge apexes. Solid lines denote exact solution: (a) pressure; (b) density; (c) Mach number, along time line $A - A'$ ($\tau = 1.125$, before shock interaction); (d) pressure; (e) density; (f) Mach number, along time line $B - B'$ ($\tau = 1.9625$, after shock interaction).

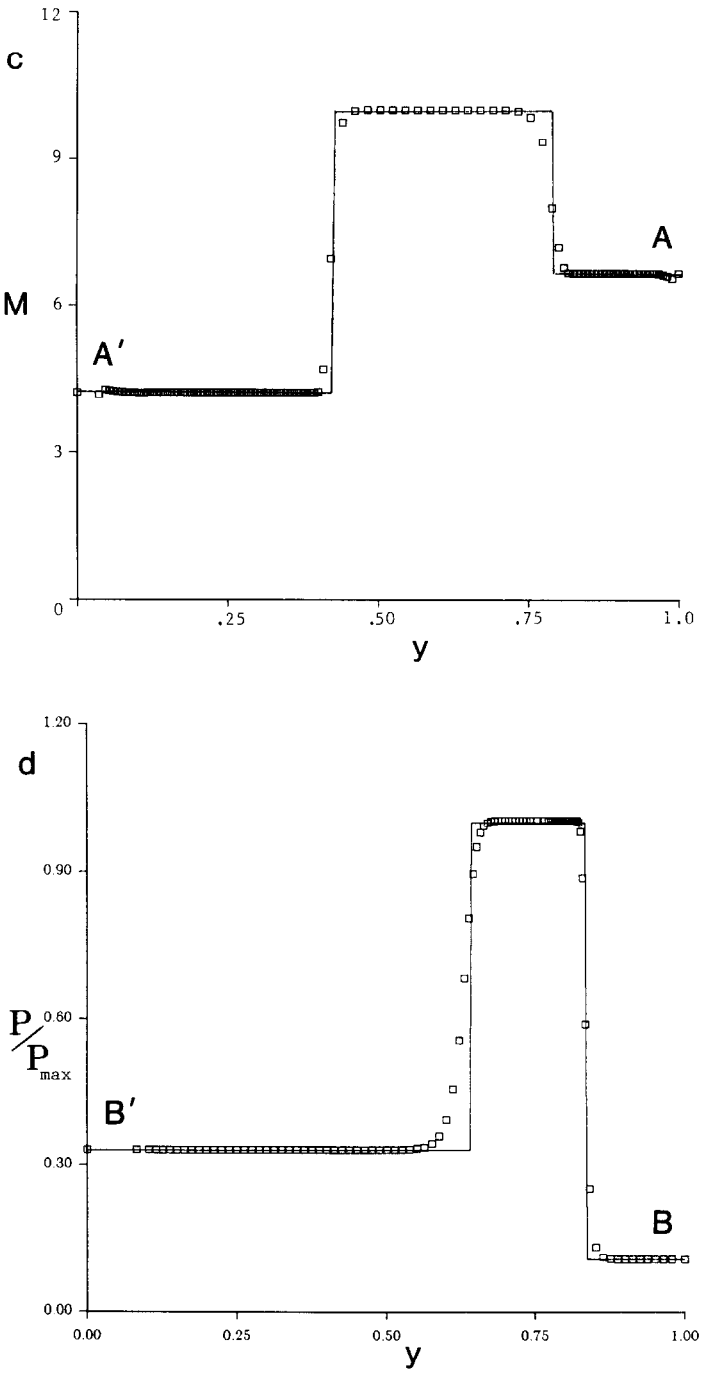

FIGURE 4 (*continued*)

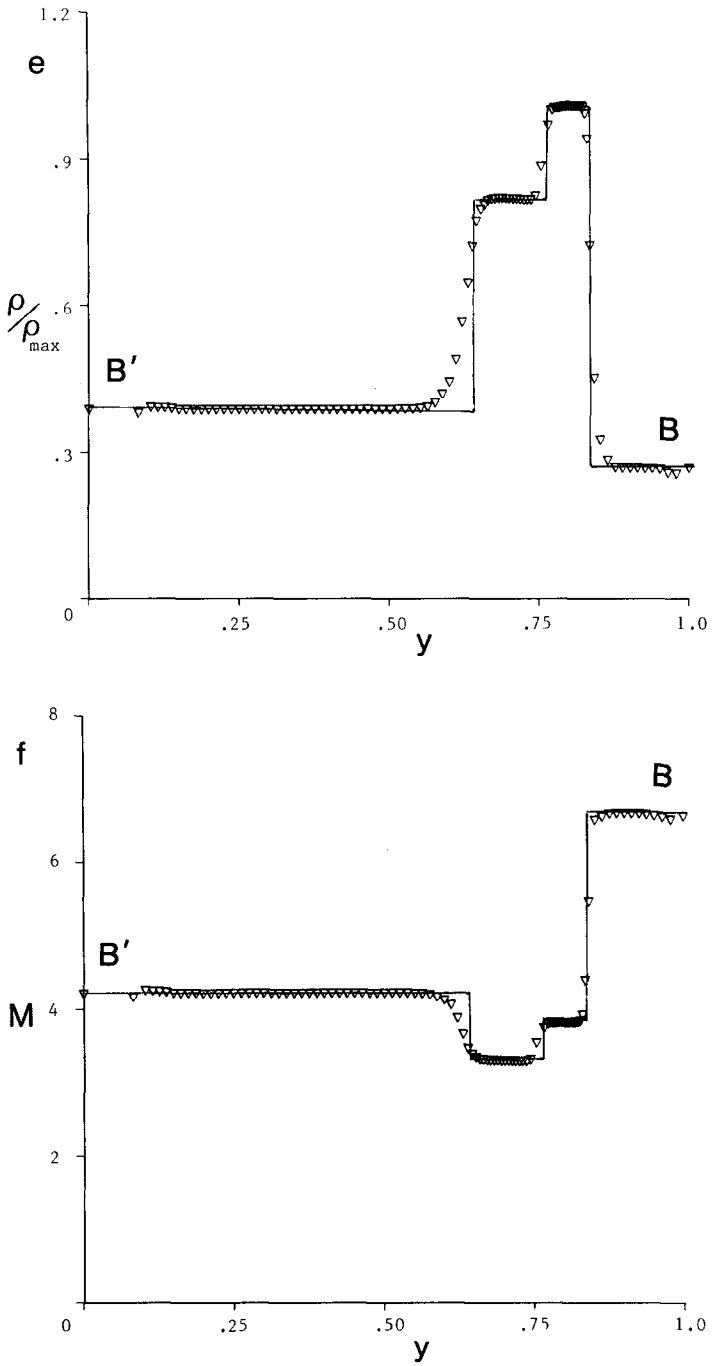

FIGURE 4 (*continued*)

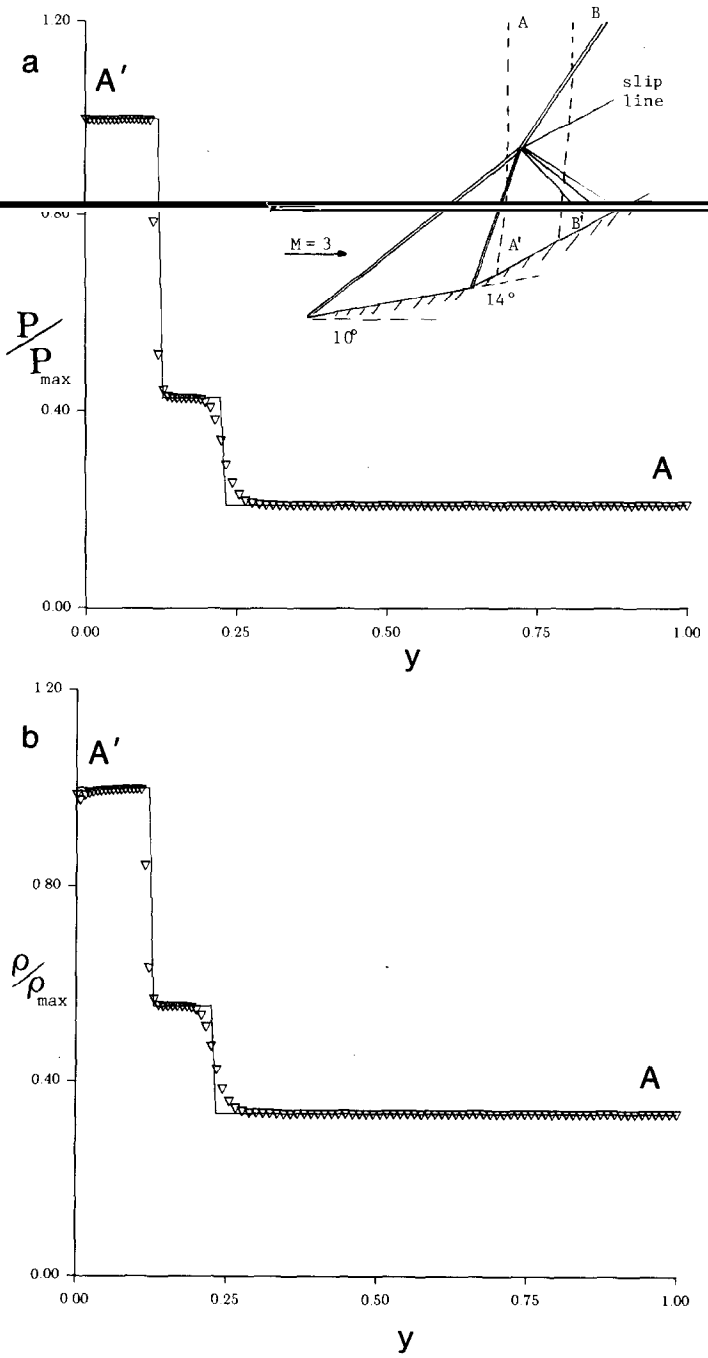

FIG. 5. Flow variables vs Eulerian co-ordinate y (normalized) along time lines before and after shock interaction. Solid lines denote the exact solution. Special procedure is employed: (a) pressure; (b) density; along time line $A - A'$ ($\tau = 0.3125$, before shock interaction); (c) pressure, (d) Mach number, along time line $B - B'$ ($\tau = 0.625$, after shock interaction).

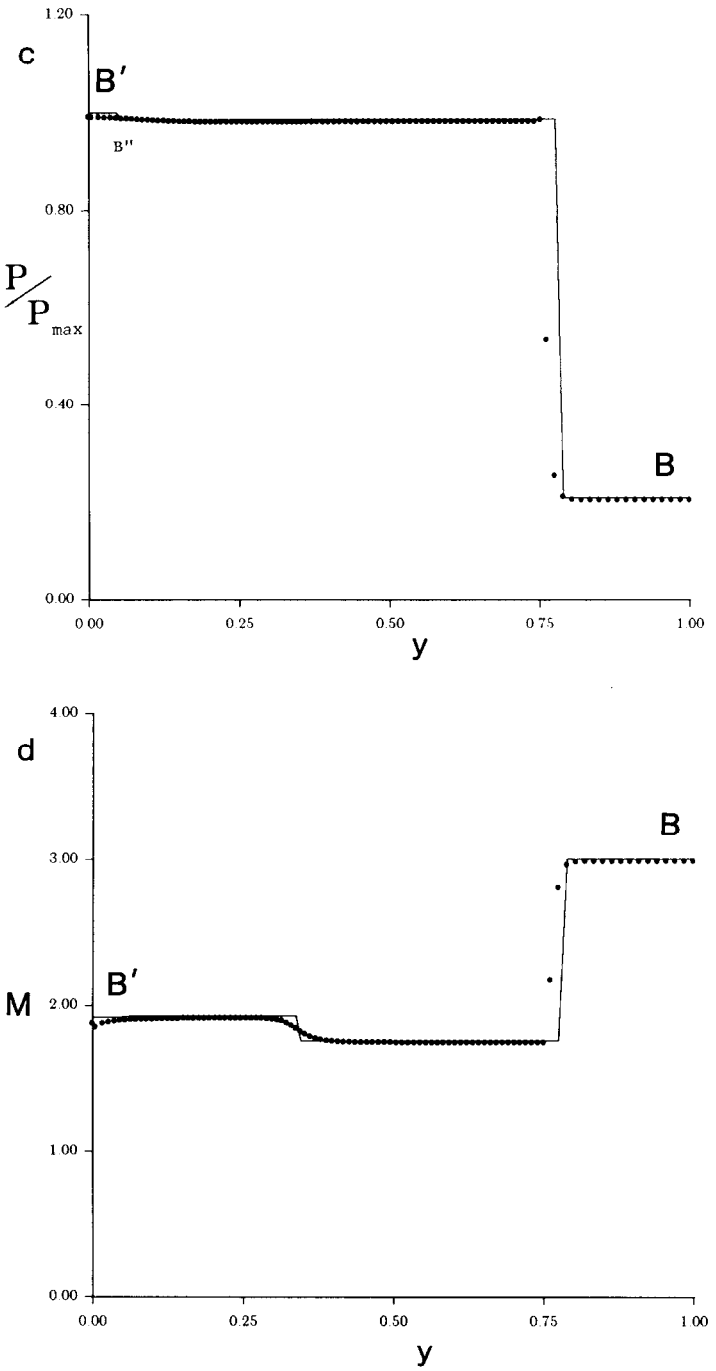

FIGURE 5 (*continued*)

V. Discussions and Conclusions

A numerical method for computing inviscid steady supersonic flow has been successfully developed by applying the Godunov (first order) scheme to the gas dynamic equations based on the new Lagrangian formulation of Hui and Van Roessel. It is fast, accurate, easy to program, and robust.

The main feature of the new Lagrangian formulation is its use of the stream function ξ and the Lagrangian time τ as independent variables, with the consequence that the body surface boundary condition is satisfied exactly on a co-ordinate line. The transformation from the cartesian co-ordinates (x, y) to the Lagrangian co-ordinates (τ, ξ) may be regarded as a form of grid generation required to render the body surface a co-ordinate line. As such it is quite a natural one, and it is interesting to note that although the streamlines and the time lines are non-orthogonal the resulting transformed equations (21) remain very simple, without the additional metric tensor terms usually arising from non-orthogonality of the transformed co-ordinates. The new Lagrangian method of computation is also self-contained without re-mapping to the Eulerian space.

It should be noted that the Lagrangian time τ is a true time variable of motion as distinguished from any-time-like variable, x say, in the Eulerian formulation.

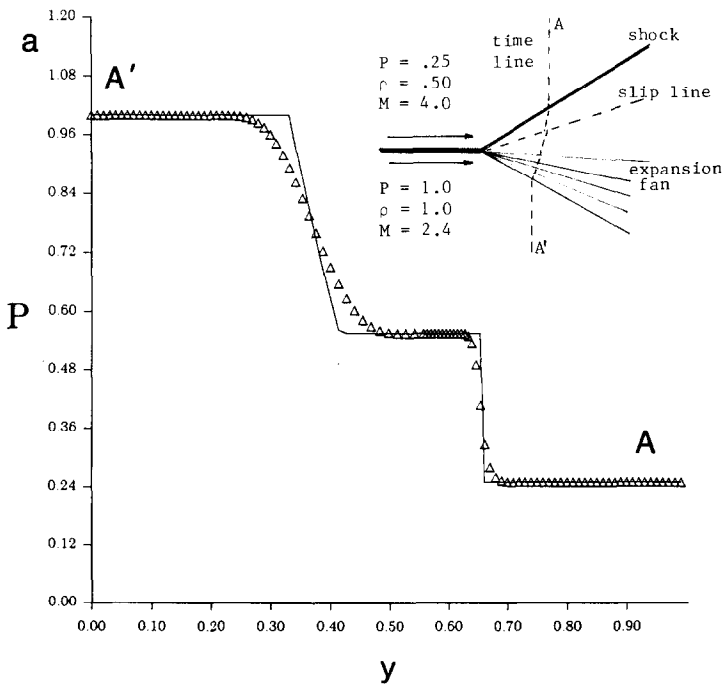

FIG. 6. Flow variables vs Eulerian co-ordinate y (normalized) along time line $A - A'$ ($\tau = 0.125$). In all figures solid lines denote the exact solution: (a) pressure; (b) density; (c) Mach number.

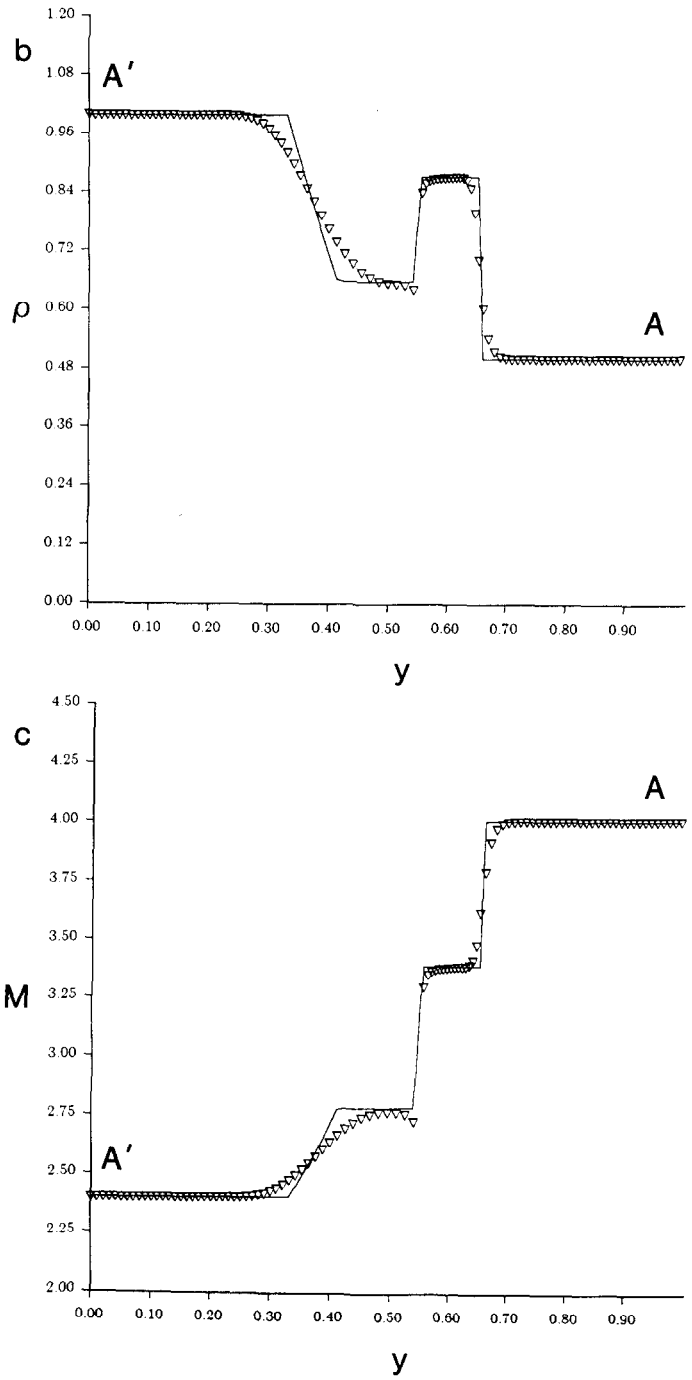

FIGURE 6 (*continued*)

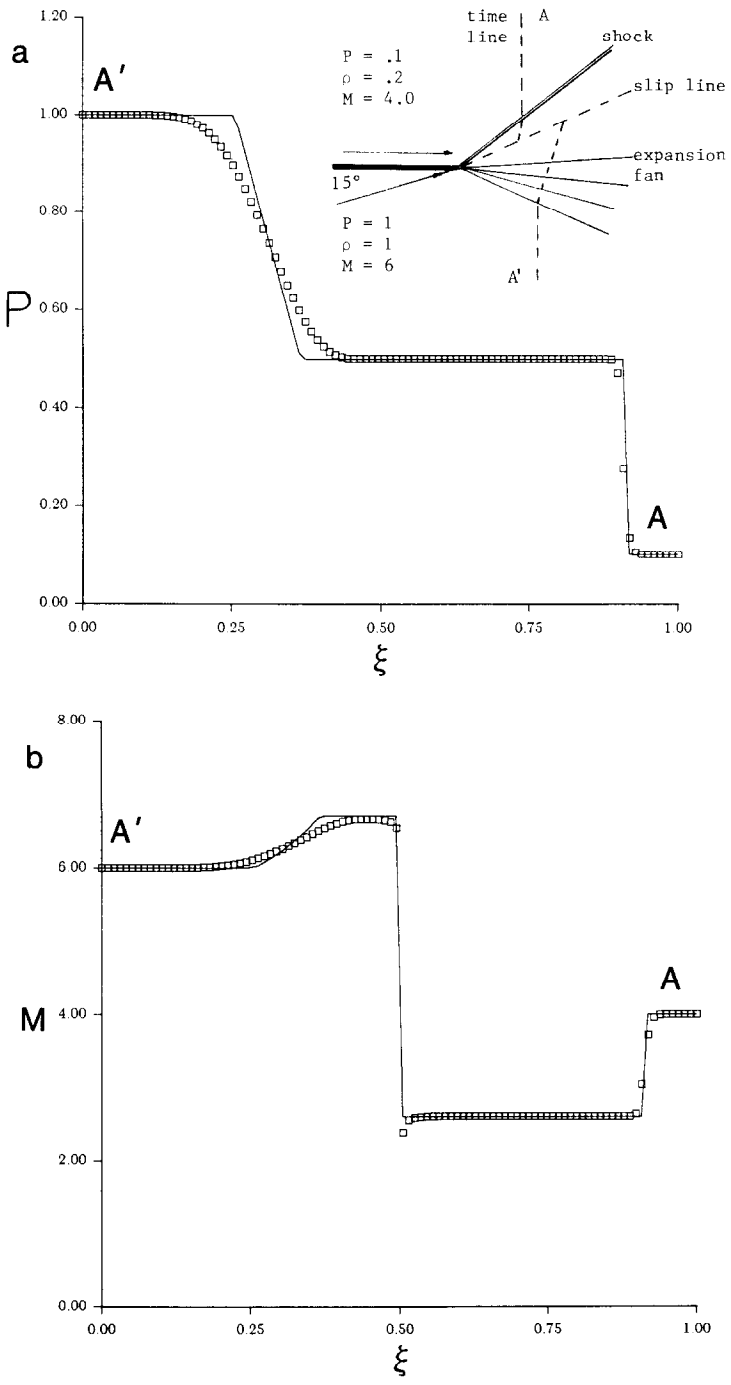

FIG. 7. Flow variables vs the Lagrangian co-ordinate ξ (normalized) along time line $A - A'$ (note that the time line is broken at the slip line). Solid lines denote exact solutions: (a) pressure; (b) Mach number.

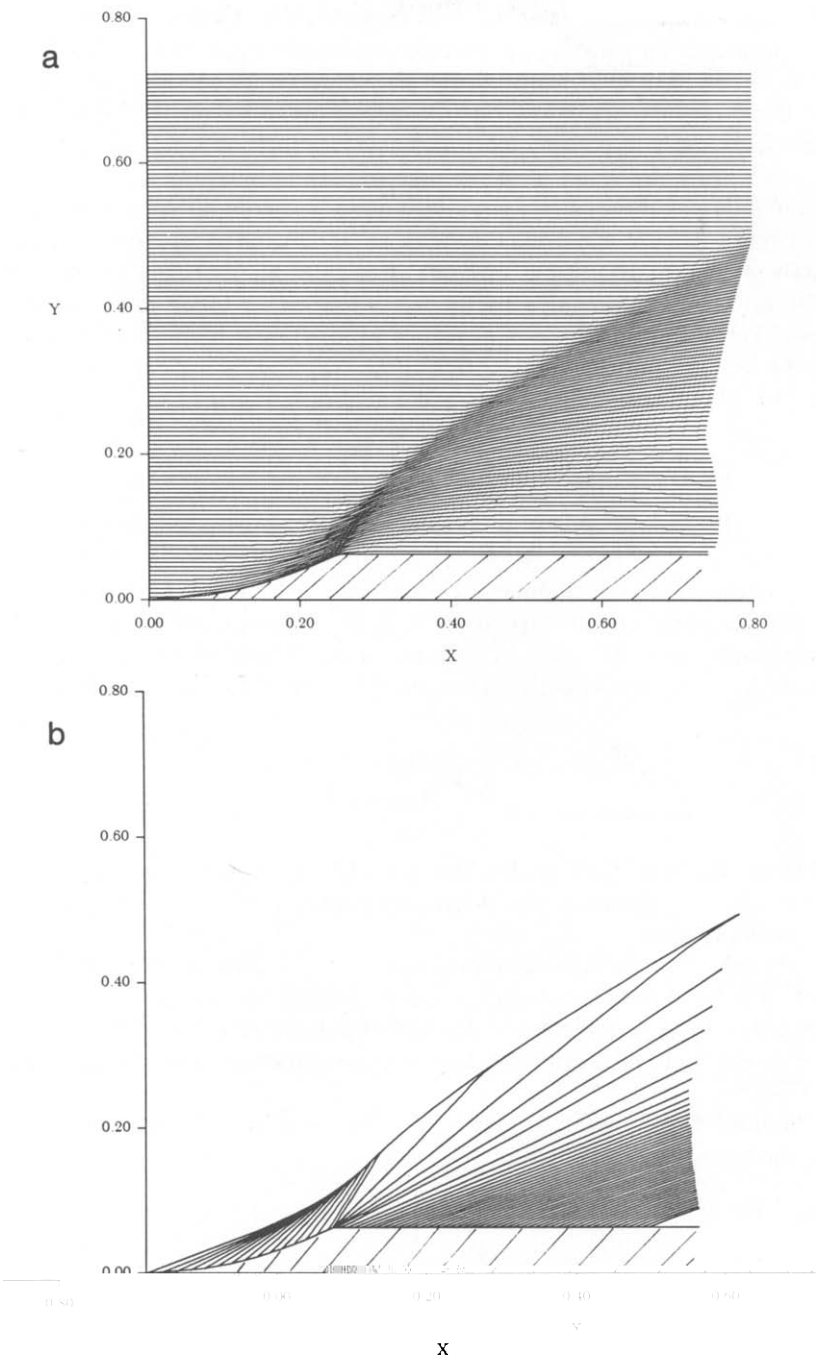

FIG. 8. (a) Computed streamlines for $M = 3$ supersonic flow past a given body. (b) Mach lines for $M = 3$ flow past a given body.

Marching in τ means following the fluid particle along its path. Thus, the computation method follows exactly the particle movement even when it crosses a shock where flow direction changes abruptly. By contrast, a time-like variable, x say, is a fixed direction in space. Consequently, marching in x does not always follow the fluid particle closely, especially when it crosses a shock; this is a source of numerical error.

In summary, in the new Lagrangian method of computation using streamlines and time lines as co-ordinate lines, the flow is followed most closely. Indeed, a cell is exactly a fluid particle and remains intact for all time. All of these probably contribute to the result of this paper that a first-order Godunov scheme based on the new Lagrangian formulation generally attains the same level of accuracy as the second order Godunov method of Glaz and Wardlaw [6] using Eulerian formulation, and is even better in resolving slip line discontinuities.

APPENDIX A: The Riemann Problem and Its Solution

As an analogue to the Riemann problem in one-dimensional unsteady flow, in the two-dimensional steady supersonic flow the Riemann problem for (21) (strictly speaking, only the first four equations of (21); the other two equations are compatibility relations) is the initial value problem with the constant data

$$\mathbf{Q} = \begin{cases} \mathbf{Q}_T, & \xi > 0 \\ \mathbf{Q}_B, & \xi < 0 \end{cases} \tag{A.1}$$

as initial condition at $\tau = 0$ for the flow state $\mathbf{Q} = (p, \rho, u, v)^{\mathrm{T}}$. The subscripts T and B denote top and bottom states, which are counterparts to the right and left states in 1D unsteady flow.

The solution of the Riemann problem is self-similar in the variable ξ/τ and consists of three types of elementary waves, namely, the oblique shock waves $(+)$, the Prandtl–Meyer expansions $(-)$ and slip lines (0). They correspond to the shocks, rarefaction waves, and contact discontinuities in 1D unsteady flow, respectively (Fig. 9).

Let $\mathbf{Q}_0$ and $\mathbf{Q}$ be the states across one of the above $+$, 0, and $-$ elementary waves, then there are three cases:

(a) The wave is a slip line. In this case we have

$$p = p_0 \equiv p^*, \qquad \theta = \tan^{-1}\left(\frac{v}{u}\right) = \theta_0 = \tan^{-1}\left(\frac{v_0}{u_0}\right) \equiv \theta^*. \tag{A.2}$$

However, the density and velocity components may jump abruptly.

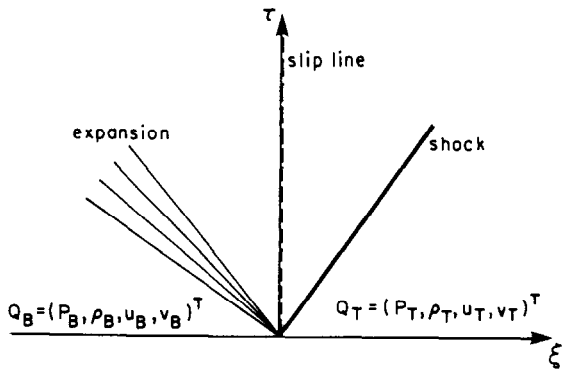

FIG. 9. Elementary waves in the solution of Riemann problem.

(b) The wave is an oblique shock ($p>p_0$). In this case we have, from the Rankine–Hugoniot oblique shock relation, for the flow deflection angle,

$$\Delta\theta = \pm\tan^{-1}\left\{\frac{\alpha-1}{\gamma M_0^2-\alpha+1}\cdot\left(\frac{2\gamma M_0^2}{(\gamma+1)\alpha+(\gamma-1)}-1\right)^{1/2}\right\}, \tag{A.3}$$

or the flow inclination

$$\theta=\theta_0\pm\Delta\theta=\theta_0\pm\tan^{-1}\left\{\frac{\alpha-1}{\gamma M_0^2-\alpha+1}\left(\frac{2\gamma M_0^2}{(\gamma+1)\alpha+(\gamma-1)}-1\right)^{1/2}\right\} \tag{A.3'}$$

and

$$\rho=\rho_0\frac{(\gamma+1)\alpha+\gamma-1}{(\gamma-1)\alpha+\gamma+1}, \tag{A.4}$$

$$M=\left[\frac{M_0^2[(\gamma+1)\alpha+\gamma-1]-2(\alpha^2-1)}{\alpha[(\gamma-1)\alpha+(\gamma+1)]}\right]^{1/2} \tag{A.5}$$

where

$$\alpha=p/p_0.$$

(c) The wave is a Prandtl–Meyer expansion. In this case we have

$$M=\left[\frac{2}{\gamma-1}\left(\frac{1+((\gamma-1)/2)M_0^2}{\alpha^{(\gamma-1)/\gamma}}-1\right)\right]^{1/2} \tag{A.6}$$

and

$$\rho=\rho_0\alpha^{1/\gamma}. \tag{A.7}$$

The flow turning angle and inclination angle are respectively

$$\Delta\theta = \mp[\nu(M) - \nu(M_0)], \qquad \theta = \theta_0 \mp [\nu(M) - \nu(M_0)], \tag{A.8}$$

where

$$\nu(M) = \sqrt{\frac{\gamma+1}{\gamma-1}} \tan^{-1}\left(\sqrt{\frac{\gamma-1}{\gamma+1}(M^2-1)}\right) - \tan^{-1}(\sqrt{M^2-1}) \tag{A.9}$$

is the Prandtl–Meyer function.

Therefore, through any state $\mathbf{Q}_0$, with $\alpha = p/p_0$ as parameter, there are two families of states connecting to $\mathbf{Q}_0$, namely, the compression states ($\alpha \geqslant 1$) and the expansion states ($\alpha < 1$). As is well known, similar to the 1D unsteady flow [14], the curves of the two families have second-order contact at $\mathbf{Q}_0$ and can be regarded as one single family. For example, in the $p-\theta$ plane, the two curves form a single smooth curve at $\mathbf{Q} = \mathbf{Q}_B$, say (Fig. 10). This forms the basis of the Newton's method in the following solution procedure for solving the Reimann problem:

(i) In the $p-\theta$ plane there are two curves that pass through the states $\mathbf{Q}_0 = \mathbf{Q}_T$ and $\mathbf{Q}_0 = \mathbf{Q}_B$; they are defined, respectively, by

$$\theta = \Phi_T(\alpha) = \begin{cases} \theta_T + \tan^{-1}\left[\dfrac{\alpha-1}{\gamma M_T^2 - \alpha + 1}\left(\dfrac{2\gamma M_T^2}{(\gamma+1)\alpha + \gamma - 1} - 1\right)^{1/2}\right], & \alpha \geqslant 1 \\ \theta_T + \nu(M_T) - \nu(M), & \alpha \leqslant 1 \end{cases} \tag{A.10}$$

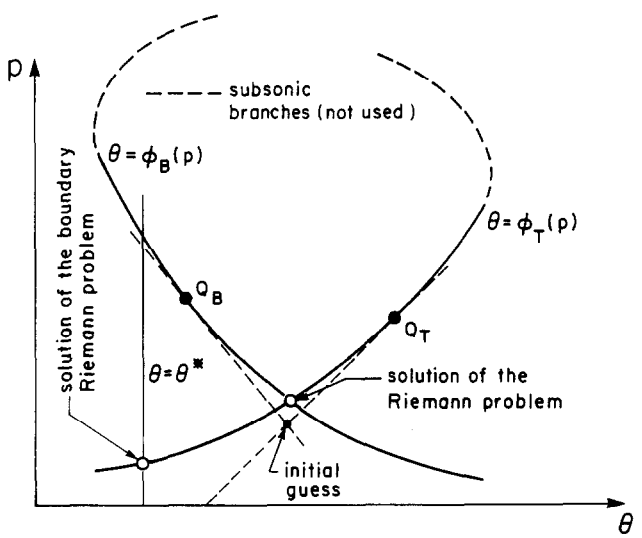

FIG. 10. Solution procedure of Riemann problem.

where $\alpha = p/p_T$, and

$$\theta = \Phi_B(\alpha) = \begin{cases} \theta_B - \tan^{-1}\left[\dfrac{\alpha - 1}{\gamma M_B^2 - \alpha + 1}\left(\dfrac{2\gamma M_B^2}{(\gamma+1)\alpha + \gamma - 1} - 1\right)^{1/2}\right], & \alpha \geqslant 1, \\ \theta_B - \nu(M_B) + \nu(M), & \alpha \leqslant 1, \end{cases} \tag{A.11}$$

where $\alpha = p/p_B$. In (A.10) and (A.11), $\nu(M)$ is given by (A.9) (with (A.6)). These curves are sketched in Fig. 10.

(ii) A standard Newton's iterative procedure is employed to find the intersect (p^*, θ^*) of the two curves. The object function in the Newton procedure is

$$f(p) = \Phi_T(p/p_T) - \Phi_B(p/p_B) \tag{A.12}$$

and the intersect of the two tangent lines passing through $\mathbf{Q}_T$ and $\mathbf{Q}_B$ is used as an initial guess to the solution. In practice we use numerical derivatives to replace the analytical ones. Usually it takes two to four iterations to converge to a tolerance $\varepsilon \leqslant 10^{-6}$. We have tested on a quite severe case: $p_T = 0.01$, $\rho_T = 0.05$, $M_T = 3.5$, and $p_B = 1.0$, $p_B = 1.0$, $M_B = 10$, it takes four iterations to convergence.

(iii) With the slip line values p^* and θ^* known, we calculate α and ρ on both sides of the slip line and then calculate the velocity components u and v, again on both sides of the slip line, using the formula

$$\begin{aligned} u &= W \cos\theta^* \\ v &= W \sin\theta^*, \end{aligned} \tag{A.13}$$

where

$$W = M\sqrt{\gamma p/\rho}. \tag{A.14}$$

These flow states on both sides of the slip line then yield the fluxes $\mathbf{F}_{j+1/2}$ for all $j \geqslant 1$.

At a solid boundary the flow tangency condition (30) must be imposed. This gives rise to the following Riemann problem, called the boundary Riemann problem, with the initial condition

$$\begin{aligned} \mathbf{Q} &= \mathbf{Q}_T, & \xi > 0 \\ \mathbf{Q} &= \mathbf{Q}_B, & \xi < 0 \\ \theta &= \theta^* = \theta_B, & \xi = 0, \end{aligned} \tag{A.15}$$

where $\mathbf{Q}_B$ is the mirror image flow of $\mathbf{Q}_T$ with respect to θ_B. In this way the

boundary condition is automatically satisfied. The solution procedure is then the same as that which we have described above.

Alternatively, by replacing Φ_B with θ_B in (A.12) we can solve for p^* directly. However, since θ_B is generally given in terms of x and hence of τ only indirectly, we need another iterative loop to achieve a better accuracy along the body surface. The details are given as follows:

(i) Assume that the state $\mathbf{Q}_T^n$ and x^n at time step n are known already. Let $\theta^* = \tan^{-1}[b'(x^n)]$.

(ii) Using u_T^n as the intitial guess for u^{n+1}, we have

$$x^{n+1} = x^n + \tfrac{1}{2}(u^n + u^{n+1})\,\Delta\tau$$

and

$$\theta^* = \tan^{-1}\{b'[x^n + \tfrac{1}{4}(u^n + u^{n+1})\,\Delta\tau]\}. \tag{A.16}$$

(iii) Solve the boundary Riemann problem with the above θ^* as the boundary condition to get a new state $\mathbf{Q}^{n+1}$, and in particular u^{n+1}.

(iv) The new u^{n+1} is then substituted back to (A.16) and a new θ^* is evaluated.

(v) We then repeat (ii)–(iv) until the tolerance between two successive θ^*s is less than a prescribed small number (say, 10^{-6}).

In our experience it usually takes one to 10 iterations to convergence.

APPENDIX B:
Special Procedure at a Sudden Turn of Body Surface

When a supersonic gas flow over a body encounters a sudden turn at the body surface, an oblique shock or a Prandtl–Meyer expansion will occur locally. The numerical scheme does not cope well with the sudden change and is likely to lead to a certain loss of acuracy (Glaz and Wardlaw [6], Noh [12], Goodman [13]). The larger the Mach number upstream of the turn and the larger the turning angle, the larger the resulting error. In order to improve the numerical accuracy downstream of the turn we impose the analytical solution at the turn locally. This special procedure is similar to the procedure used by Glaz and Wardlaw [6]; the details are described as follows:

(1) in the case of a sudden compression. (The following procedure is that of Glaz and Wardlaw [6].)

(a) Adjust time step size $\Delta\tau$ so that the turning corner is hit exactly by a mesh time line (at "0" in Fig. 11).

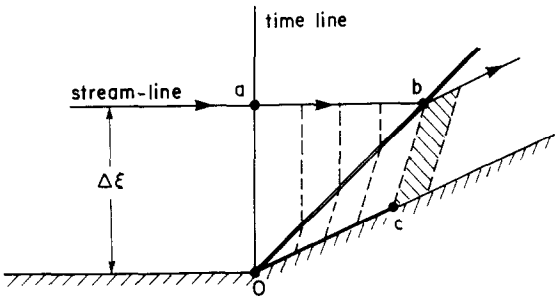

FIG. 11. Special procedure for compression turn.

(b) Store the flow state $\mathbf{Q}_u$ and $\mathbf{E}_u$ upstream of "0." Then use the Rankine–Hugoniot relation to calculate the exact downstream state $\mathbf{Q}_d$.

(c) In the physical plane when the wall (boundary) cell still lies across the shock, temporarily give up using the boundary Riemann solver and assign $\mathbf{Q}_d$ as the wall flux (along "0C" in Fig. 11) in the numerical procedure.

(d) When the wall cell is completely downstream of the shock, assign the state $\mathbf{Q}_d$ to the wall cell (shaded area in Fig. 11), and use (21) and the divergence theorem to calculate $\mathbf{E}_d$ along the quadrilateral *oabc*. Now terminate the special procedure and resume the normal one.

(2) in the case of sudden expansion.

(a) Adjust time step size so that the turning corner is hit exactly by a mesh time line (at "0" in Fig. 12).

(b) Store the flow state $\mathbf{Q}_u$ and $\mathbf{E}_u$ upstream of "0" and use $\mathbf{Q}_u$ to calculate the exact Prandtl–Meyer flow $\mathbf{Q}_d$.

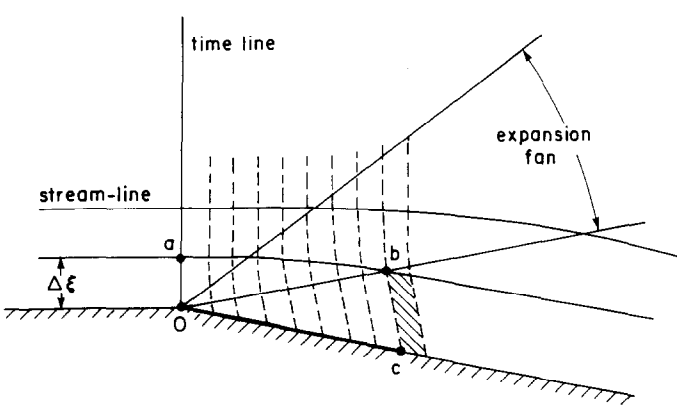

FIG. 12. Special procedure for expansion turn.

(c) Use Appendix C to check the locations of cell centers along a time line. Once a cell center enters the expansion fan or the uniform region behind it, we temporarily disregard all the local Riemann solvers and simply assign the exact state $\mathbf{Q}$ to that cell in the numerical procedure until the wall cell (shadded one in Fig. 12) first entirely enters the uniform region downstream of the expansion fan.

(d) Use (21) and the divergence theorem to evaluate $\mathbf{E}_d$ along the curved quadrilateral "*oabc*" for continuing computation, and the special procedure is terminated.

Our special procedure in (2) is somewhat different from that in [6] (Glaz and Wardlaw) and yields satisfactory numerical results.

APPENDIX C:
Analytical Solutions for Elementary Waves in the $\tau - \xi$ Formulation

In this appendix we present the exact analytical solutions for elementary waves, namely, oblique shock wave and Prandtl–Meyer expansion in the $\tau - \xi$ formulation so that we can compare our numerical results directly with the exact results rather than going through the remapping to the Eulerian space; the remapping can cause additional errors. The problem is as follows: with a given free stream state $\mathbf{Q}_\infty$ and given any (τ, ξ) coordinates in the Lagrangian system find the state $\mathbf{Q}$ at the location (τ, ξ).

(1) In the case of an oblique shock, from the geometrical relation in Fig. 13 the solution is simple: if $\xi \geqslant u_\infty \tau \cot \beta_s$, the point P falls in Region I, and

$$\mathbf{Q} = \mathbf{Q}_\infty,$$

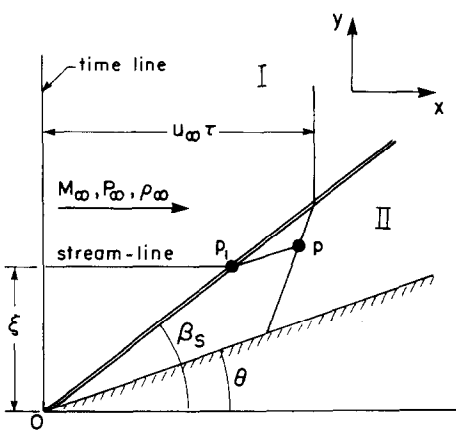

FIG. 13. Analytical solution for an oblique shock in $\tau - \xi$ formulation.

where β_s, u_∞, and $\mathbf{Q}_\infty$ are respectively the oblique shock angle, free stream velocity, and the free stream state in I.

If $\xi < u_\infty \tau \cot \beta_s$, the point P falls in Region II and

$$\mathbf{Q} = \mathbf{Q}_s,$$

where $\mathbf{Q}_s$ is the constant state behind the oblique shock.

(2) In the case of a Prandtl–Meyer expansion flow the following notations are used (see Fig. 14):

M_∞ free steam Mach number,

a_∞—free stream sound speed,

$\mu_\infty = \sin^{-1}(1/M_\infty)$—Mach angle,

$\lambda = \sqrt{(\gamma-1)/(\gamma+1)}$, where γ $(=1.4)$ is the ratio of specific heats,

$\theta_\infty = (1/\lambda)\tan^{-1}(\lambda\sqrt{M_\infty^2 - 1})$.

Let $\Delta = \theta_\infty + \mu_\infty - \pi/2$, then (see Hui [15]),

$$\begin{aligned} u &= c \sin \lambda(\theta + \Delta), \\ v &= c\lambda \cos \lambda(\theta + \Delta), \end{aligned} \tag{A.17}$$

where u is the radial velocity component and v the transversal volocity component (Fig. 14), and

$$c = a_\infty \sqrt{M_\infty^2 + 2/(\gamma - 1)}. \tag{A.18}$$

We also define the initial time line $\tau = 0$ as the vertical line passing through 0 (the dashline in Fig. 14). Then

(i) in Region I, where the given τ and ξ satisfy $\tau \leqslant \tau_0 = \xi\sqrt{M_\infty^2 - 1}/u_\infty$, we have exactly the free steam uniform flow.

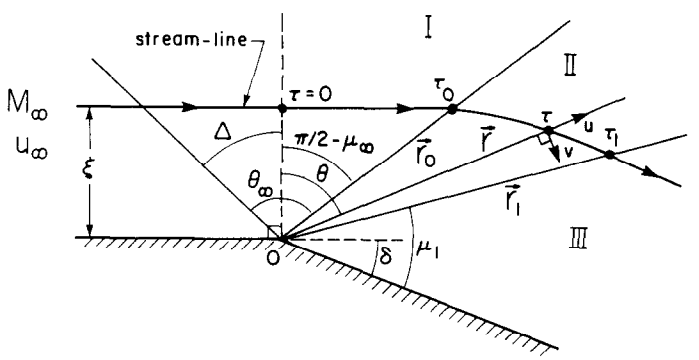

FIG. 14. Analytical solution of Prandtl–Meyer flow in $\tau - \xi$ formulation.

(ii) in Region II, i.e., in the expansions fan for which $\tau_0 \leqslant \tau \leqslant \tau_1$, where τ_1 is given in (A.25). Let (r, θ) be the polar co-ordinates of a fluid particle then, the equation of its streamline is (Fig. 14)

$$\frac{dr}{u} = \frac{r\, d\theta}{v} = d\tau. \tag{A.19}$$

Recalling (A.17) we find

$$\frac{dr}{r} = \frac{u}{v} d\theta = \frac{1}{\lambda} \tan \lambda(\theta + \Delta) d(\theta + \Delta),$$

which integrates to give

$$r = K \cos^{-1/\lambda^2} \lambda(\theta + \Delta), \tag{A.20}$$

where $K = K(\xi)$ is a constant along a given streamline. To determine K, we recall that $\theta + \Delta = \theta_\infty$ and, $r = \xi / \sin \mu_\infty = M_\infty \xi_b$ at $\theta = \theta_0 - \pi/2 - \mu_\infty$; hence

$$K = K(\xi) = M_\infty \xi \cos^{1/\lambda^2}(\lambda \theta_\infty). \tag{A.21}$$

From (A.19),

$$d\tau = \frac{r}{v} d\theta = \frac{K}{c\lambda} \cos^{-2\gamma/(\gamma-1)}[\lambda(\theta + \Delta)]\, d\theta. \tag{A.22}$$

In particular, if $\gamma = 1.4$, we get

$$d\tau = \frac{K}{c\lambda^2} \frac{d\lambda(\theta + \Delta)}{\cos^7[\lambda(\theta + \Delta)]}. \tag{A.23}$$

Let

$$A = A(\xi) = \frac{K(\xi)}{c\lambda^2} = \frac{M_\infty \xi \cos^{(\gamma+1)/(\gamma-1)}(\lambda \theta_\infty)}{a_\infty \sqrt{M_\infty^2 + (2/(\gamma-1))}} \frac{\gamma + 1}{\gamma - 1},$$

then (A.23) can be integrated to give

$$\tau = \tau_0 + A \int_{\theta_0}^{\theta} \frac{d\lambda(\theta + \Delta)}{\cos^{2\gamma/(\gamma-1)}[\lambda(\theta + \Delta)]}; \tag{A.24}$$

in particular,

$$\tau_1 = \tau_0 + A \int_{\theta_0}^{\theta_1} \frac{d\lambda(\theta + \Delta)}{\cos^{2\gamma/(\gamma-1)}[\lambda(\theta + \Delta)]}, \tag{A.25}$$

where θ_1, given in (A.29), is the angle between the time line $\tau = 0$ and the last Mach line of the Prandtl–Meyer expansion fan.

With (τ, ξ) given, $\theta = \theta(\tau, \xi)$. In the computation an inverse function of (A.24) is needed to determine the flow. This can be obtained by a Newton iterative procedure as follows: Let

$$f(\theta) = \tau_0 + A(\xi) \int_{\theta_0}^{\theta} \frac{d\lambda(\theta + \Delta)}{\cos^{2\gamma/(\gamma-1)}[\lambda(\theta + \Delta)]}.$$

Then define the object functions as

$$\phi(\theta) = \tau - f(\theta);$$

hence

$$\phi'(\theta) = -f'(\theta) = -A(\xi) \frac{\lambda}{\cos^{2\gamma/(\gamma-1)}[\lambda(\theta + \Delta)]}.$$

The Newton procedure is then carried out as

$$\theta^{(n+1)} = \theta^{(n)} + \frac{\cos^{2\gamma/(\gamma-1)}[\lambda(\theta^{(n)} + \Delta)]}{\lambda A(\xi)} \phi(\theta^{(n)}) \tag{A.26}$$

where, as usual, the superscript (n) denotes the nth iteration. $\theta^{(0)} = (\theta_0 + \theta_1)/2$ can be used as initial guess and the integral $\int_{\theta_0}^{\theta} (d\lambda(\theta + \Delta)/\cos^{2\gamma/(\gamma-1)}[\lambda(\theta + \Delta)])$ can be calculated analytically for $\gamma = 1.4$ or numericaly by Simpson's rule.

In the expansion fan once θ is determined for the given (τ, ξ), the usual Prandtl–Meyer flow formulas are employed:

$$\begin{aligned} M(\theta) &= 1 + \frac{1}{\lambda^2} \tan^2[\lambda(\theta + \Delta)], \\ p &= p_\infty \left[\frac{1 + ((\gamma-1)/2) M_\infty^2}{1 + ((\gamma-1)/2) M^2(\theta)} \right]^{\gamma/(\gamma-1)} \\ \rho &= \rho_\infty \left[\frac{1 + ((\gamma-1)/2) M_\infty^2}{1 + ((\gamma-1)/2) M^2(\theta)} \right]^{1/(\gamma-1)}. \end{aligned} \tag{A.27}$$

(iii) in Region III, i.e., $\tau \geqslant \tau_1$, the flow is uniform. We apply the usual Prandtl–Meyer relations. First, we calculate the Mach number M_1 from the equation

$$\nu(M_1) = \delta + \nu(M_\infty), \tag{A.28}$$

where δ is the flow turning angle (Fig. 14). The inversion of the Prandtl–Meyer

function $\nu(M_1)$ to yield M_1 is done by a Newton iterative procedure. We then calculate

$$\theta_1 = \frac{\pi}{2} + \delta - \sin^{-1}\left(\frac{1}{M_1}\right) \tag{A.29}$$

and τ_1 is evaluated from (A.25). When $\tau \geqslant \tau_1$ the flow is in the Region III with $M \equiv M_1$ and p, ρ from (A.27).

ACKNOWLEDGMENTS

This research was supported by a grant from the Natural Science and Engineering Research Council of Canada awarded to W. H. Hui and an NSERC Postdoctoral Fellowship to C. Y. Loh. The authors thank the reviewers for their valuable comments. The computations for this paper were carried out using the Cray X-MP2 computer at the Ontario Center for Large Scale Computation.

REFERENCES

1. P. WOODWARD AND P. COLLELLA, *J. Comput. Phys.* **54**, 115 (1984).
2. A. RIZZI AND B. ENGQUIST, *J. Comput. Phys.* **72**, 1 (1987).
3. W. G. SUTCLIFFE, "BBC Hydrodynamics," Lawrence Livermore National Lab., Report UCID-17013, 1973 (unpublished).
4. P. COLLELLA AND P. WOODWARD, *J. Comput. Phys.* **54**, 14 (1984).
5. B. VAN LEER, *J. Comput. Phys.* **32**, 101 (1979).
6. H. M. GLAZ AND A. B. WARDLAW, *J. Comput. Phys.* **58**, 157 (1985).
7. W. H. HUI AND H. VAN ROESSEL, in *NATO AGARD Symposium on Unsteady Aerodynamics —Fundamentals and Application to Aircraft Dynamics, Göttingen, West Germany, 6–9 May, 1985*, S1, CP-386 (AGARD, 1985).
8. H. J. VAN ROESSEL AND W. H. HUI, *J. Appl. Math. Phys. (ZAMP)* **40**, 677 (1989).
9. H. J. VAN ROESSEL AND H. W. HUI, Unsteady three dimensional Newton–Busemann flow using material functions, *Intern. J. Nonlinear Mech.*, in press.
10. A. HARTEN, *J. Comput. Phys.* **49**, 357 (1983).
11. A. HARTEN, B. ENGQUIST, AND S. OSHER, *J. Comput. Phys.* **71**, 231 (1987).
12. W. F. NOH, Lawrence Livermore National Lab., Report UCRL-52112, 1976 (unpublished).
13. J. GOODMAN, Center for Pure and Applied Mathematics, U. C. Berkeley, Report PAM-99, 1982 (unpublished).
14. E. BECKER, *Gas Dynamics* (Academic Press, New York/London, 1968).
15. W. H. HUI, *J. Appl. Math. Phys. (ZAMP)* **29**, 414 (1978).